energies

MDPI

Article

Influence of Battery Life Degradation on PV Battery Capacity Configuration in Urban Industrial Park in Shanghai

Yujie Xie [1], Zhengrong Li [2], Tianzhe Shi [1], Qianjin Huang [1] and Han Zhu [2,*]

[1] School of Mechanical Engineering, Tongji University, Shanghai 200092, China; xyjavon@tongji.edu.cn (Y.X.); shitianzhe@tongji.edu.cn (T.S.); 2530609@tongji.edu.cn (Q.H.)
[2] College of Architecture and Urban Planning, Tongji University, Shanghai 200092, China; lizhengrong@tongji.edu.cn
* Correspondence: zhuhan@tongji.edu.cn

Abstract

Urban industrial parks have high electricity demand, and rooftop photovoltaic (PV)-battery systems can help reduce grid dependence and carbon emissions. However, battery degradation affects battery replacement timing and long-term economic performance, which should be considered in capacity sizing. This study proposes a degradation-aware techno-economic sizing method for rooftop PV-battery systems in urban industrial parks. GIS-based rooftop assessment, EnergyPlus load modeling, TRNSYS system simulation, battery SOH tracking, and NPV evaluation were integrated into one framework. A case study was conducted for an urban industrial park in Shanghai, China. The usable rooftop area was estimated as 113,208 m^2, corresponding to a PV capacity of approximately 18,765 kWp. The annual PV generation was 24.7 GWh, accounting for 24.7% of the park's annual electricity demand. Battery capacities from 5000 to 40,000 kWh were evaluated. The results show that increasing battery capacity improves load shifting and reduces direct grid supply, but the marginal benefit gradually decreases. The maximum NPV is obtained at 30,000 kWh, with an NPV of 128.36 million CNY, a simple payback period of 4.6 years, and a discounted payback period of 6.0 years. The rooftop PV system achieves a 25-year CO_2 emission reduction of approximately 335,967 tCO_2 after considering PV degradation. Sensitivity analyses show that BES cost, tariff spread, and discount rate are key factors affecting the recommended capacity.

Keywords: rooftop PV; PV battery system; potential; technical and economic feasibility; battery life degradation

Check for updates

Academic Editor: Santiago Silvestre

Received: 29 April 2026
Revised: 11 June 2026
Accepted: 17 June 2026
Published: 24 June 2026

Copyright: © 2026 by the authors. Licensee MDPI, Basel, Switzerland. This article is an open access article distributed under the terms and conditions of the Creative Commons Attribution (CC BY) license.

1. Introduction

Urban industrial parks are important carriers of economic activity and are also areas with intensive electricity consumption and carbon emissions. With the increasing pressure of climate change and carbon neutrality targets [1,2], many countries have proposed carbon neutrality agendas, and China has pledged to peak carbon emissions by 2030 and achieve carbon neutrality by 2060 [3,4]. Industrial parks are therefore important objects for low-carbon energy transition because their remaining operating life and concentrated energy demand are closely related to future carbon emissions [5–7]. Reducing grid electricity dependence and improving local renewable-energy utilization in industrial parks are essential for achieving carbon-reduction objectives [8].

Rooftop photovoltaic (PV) systems are suitable for urban industrial parks because they can use existing building roofs without occupying additional land resources. PV

has been widely recognized as a promising renewable energy technology for reducing fossil-energy consumption and CO_2 emissions [9,10]. Rooftop PV systems can also be integrated with buildings and consumed locally at the community or park scale [11,12]. Previous studies have evaluated rooftop PV potential from geographic, technical, economic, and environmental perspectives [13]. For example, rooftop PV feasibility and economic performance have been analyzed for residential buildings, campuses, and urban building stocks [14–16]. Recent studies have further improved rooftop PV assessment by considering detailed rooftop layout and building-cluster characteristics [17]. However, these studies mainly focus on PV potential itself, while the coupled operation of PV generation, building load, battery storage, degradation, and long-term economic performance is not always fully represented.

Because solar energy is intermittent and variable, rooftop PV systems are often combined with battery energy storage systems (BESS) to improve local consumption and load-shifting capability [18]. With the decline in battery costs and the development of electric-vehicle-related technologies, battery storage has become an increasingly important option for renewable-energy integration [19,20]. Many studies have investigated the techno-economic performance of PV-battery systems under different load profiles, regions, and financial conditions [21–23]. These studies demonstrate the potential economic value of PV-battery systems, but many of them still use fixed battery lifetimes or simplified replacement assumptions, which may not reflect the influence of cycling behavior on long-term battery degradation.

Battery degradation has a direct influence on the technical and economic performance of PV-battery systems [24]. Previous studies have discussed lithium-ion battery degradation mechanisms and health-estimation methods [25–28]. More recently, degradation-aware PV-battery sizing and operation models have been developed. Wu et al. [29] proposed a PV-battery capacity optimization model considering long-term battery degradation. Zhang et al. [30] studied energy storage sharing schemes in industrial parks while considering battery degradation. Yoshida et al. [31] evaluated the impact of battery degradation on grid-connected PV-battery operation. Recent studies have also incorporated BESS degradation into sizing and energy-management optimization [32,33]. These works confirm that battery degradation affects optimal capacity, operation cost, and replacement timing.

Nevertheless, existing degradation-aware sizing studies are often formulated as mixed-integer linear programming, mixed-integer nonlinear programming, or other mathematical optimization problems. These methods are powerful for identifying optimal capacities and dispatch schedules, but they usually require simplified component models, linearized degradation functions, representative time periods, or fixed degradation-cost coefficients to maintain computational tractability [34]. Multi-year stochastic optimization can include uncertainty and degradation effects, but its computational burden increases when long-term financial variables and detailed operational constraints are considered [35]. Therefore, the dynamic interaction among PV output, building load, SOC constraints, available battery capacity, SOH evolution, and degradation-driven replacement timing may not be fully captured in a reproducible park-scale simulation workflow.

For urban industrial parks, this limitation is particularly important. The recommended battery capacity depends not only on the annual energy balance, but also on how the battery is charged and discharged under time-of-use tariffs, how frequently it reaches SOC limits, how cycling intensity changes with battery size, and how battery degradation affects available capacity and replacement cost. Recent research on urban industrial building rooftop PV-storage systems has emphasized the importance of considering device degradation and life-cycle performance [36]. However, there is still a need for a practical simulation-based framework that links rooftop suitability assessment, building load estimation, dynamic PV-

battery operation, degradation-aware SOH tracking, and NPV-based capacity evaluation for a specific urban industrial park.

To address this gap, this study proposes a degradation-aware techno-economic sizing method for rooftop PV-battery systems in urban industrial parks. Unlike optimization-only approaches that rely mainly on simplified mathematical formulations, this study adopts a TRNSYS-based dynamic simulation combined with parametric battery capacity evaluation. The purpose is not to replace MILP or MINLP optimization methods, but to provide a complementary simulation-based workflow that can explicitly represent PV generation, building load, SOC-constrained battery operation, battery SOH tracking, and degradation-aware capacity updates. GIS-based rooftop suitability assessment is used to estimate available PV installation area; EnergyPlus is used to generate representative building electricity demand profiles; and TRNSYS is used to simulate system operation under local time-of-use tariff conditions. NPV is used as the main economic evaluation indicator, and sensitivity analyses are conducted to examine the effects of BES cost, tariff spread, discount rate, export price, and battery degradation coefficient.

Accordingly, this study mainly focuses on three aspects. First, a park-scale simulation-based evaluation workflow is established by combining GIS rooftop assessment, EnergyPlus load modeling, TRNSYS dynamic simulation, battery SOH tracking, and NPV calculation. Second, an equivalent-full-cycle-based battery degradation model is implemented in TRNSYS through user-defined equations to evaluate available battery capacity under different battery capacities. Third, a Shanghai industrial park case is used to examine rooftop PV potential, PV-battery operation, battery degradation, economic performance, carbon emission reduction, and parameter sensitivity under local tariff conditions.

2. Methodology

This paper adopts the TRNSYS 18.0 software for simulating photovoltaic battery systems. TRNSYS software is widely utilized in both commercial and scientific domains, owing to its capability to account for various factors such as climatic conditions, system characteristics, and control strategies [37,38]. This enables it to deliver precise predictions of energy system performance, approaching real-world simulations. Moreover, TRNSYS offers extensive extensibility, empowering users to customize components and modules to meet the specific requirements of diverse systems [39]. Within the utilized software, selected components and connections are utilized to construct the system structure in a user-friendly graphical environment.

The feasibility calculation for the system installation in this park encompasses four steps (Figure 1). Initially, building contours and heights are obtained using BIGMAP data and GIS methods, while weather data is sourced from Meteonorm 8.0. Additionally, building electricity demand is estimated using EnergyPlusV23-2-0. Subsequently, the usable rooftop area is determined. Thirdly, the TRNSYS model is developed. Furthermore, the battery life degradation model and time-of-use electricity price control model are integrated into the battery module (Type47a) and the regulator/inverter module (Type48b). Finally, the energy results and economic benefits of the system are calculated.

2.1. Suitable Area Calculation

The vector data of the building rooftop boundaries in BIGMAP and the buildings under construction and those unsuitable for installing PV panels are excluded. When extracting vector data, there may be omissions that require manual correction and adjustment. ArcGIS 10.8 was used to identify the total rooftop area A_{total} in the park.

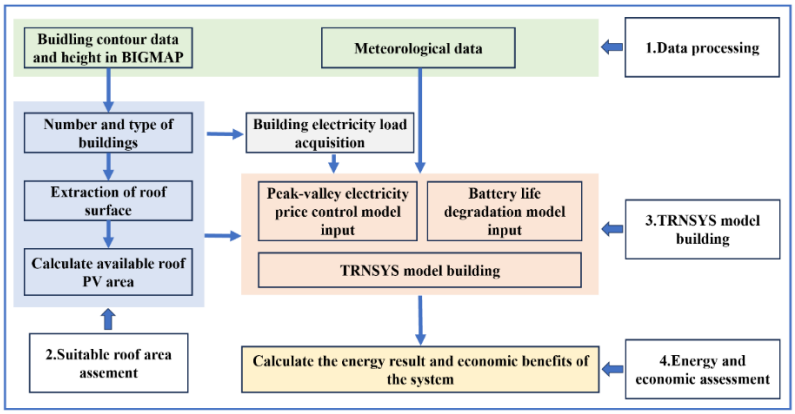

Figure 1. Flowchart of the proposed method.

The individual roofs exhibit significant differences in characteristics. There are some obstructing elements on the rooftops, including (a) shadows originating from other parts of the roof, neighboring buildings, and trees; (b) Occupancy of equipment, such as elevator shafts, parapets, cooling towers, fans, and so on; (c) the installation of PV panels [40,41]. Since these obstructing elements are not depicted when getting vector data of the building rooftop boundaries, the reduction coefficients η_{roof} need to be considered. The useable rooftop area can be calculated by Equation (1) [42]:

$$A_{tot,useable} = \eta_{roof} \times A_{total} \quad (1)$$

Different building types have different rooftop utilization conditions because of rooftop obstacles, equipment occupation, installation spacing requirements, and shading from surrounding buildings, rooftop structures, and vegetation. Therefore, a rooftop reduction coefficient, η_{roof}, was introduced to estimate the usable rooftop area for PV installation. The coefficient represents the reduction in installable rooftop area caused by these factors. The values of η_{roof} for different building types were determined based on previous rooftop PV potential studies [43] and visual interpretation of the building roofs in the study area. The adopted coefficients are listed in Table 1.

Table 1. Rooftop PV reduction coefficients for different building types.

Building Type	η_{roof}
Office buildings	0.53
Commercial buildings	0.33
Residential buildings	0.40
School buildings	0.42

2.2. Electrical Demand Profiles

Hourly electrical demand profiles were generated using EnergyPlus because measured electricity data for individual buildings in the park were not available. Four representative building archetypes were considered: office, commercial, school, and residential buildings. The EnergyPlus models included lighting and plug/equipment electricity consumption, while heating-related electricity demand from heat pumps or electric heaters was excluded [44]. The hourly electricity profile of each archetype was scaled by its corresponding floor area in the park and then aggregated to obtain the park-level load profile used as the input to TRNSYS. The specific floor areas and internal load assumptions used in the Shanghai case study are provided in Section 3.1.

2.3. Battery Life Degradation Model

2.3.1. Aging Model

Battery life degradation is mainly affected by operating temperature, cumulative cycling intensity, depth of discharge, and charge–discharge rate. In this study, battery cycle aging is estimated using a semi-empirical cycle-life model for graphite-$LiFePO_4$ cells based on the Arrhenius equation and cumulative charge throughput. Under a specified discharge-rate condition, the cumulative capacity loss of a battery cell can be expressed as [45]:

$$Q_{\text{loss}} = A \exp\left(\frac{-E_a}{RT}\right)\mu^z \tag{2}$$

where Q_{loss} represents the cumulative battery capacity fade (%); z is the power-law factor; A is the pre-exponential factor; R is the molar gas constant, 8.314 J/(mol K); E_a is the activation energy (J/mol); T is the absolute battery temperature (K); and μ^z represents chemical time (h). Following Wang et al. [45], μ^z can be replaced by the cumulative Ah-throughput, which links battery degradation with the cycle number and depth of discharge. Therefore, Equation (2) can be rewritten as Equation (3).

$$Q_{\text{loss}} = A \exp\left(\frac{-E_a}{RT}\right){A_h}^z \tag{3}$$

$$A_h = Q_{cell} \times h \times n \tag{4}$$

where A_h is the cumulative Ah-throughput (Ah); Q_{cell} is the rated cell capacity (Ah); h is the depth of discharge for each cycle; and n is the number of cycles.

For the graphite-$LiFePO_4$ cells tested by Wang et al. [45], the rated cell capacity was set to 2 Ah. Under the C/2 discharge-rate condition, the fitted parameters are E_a = 31,500 J/mol, A = 30,330, Q_{cell} = 2 Ah, and z = 0.552.

Therefore, the original cell-level degradation model is:

$$Q_{\text{loss}} = A \exp\left(\frac{-E_a}{RT}\right)(Q_{cell} \times h \times n)^z \tag{5}$$

For a park-scale battery energy storage system, directly calculating the total Ah-throughput is inconvenient because the system-level simulation is based on power in kW and energy in kWh. Therefore, the equivalent full cycle number is introduced to characterize the cumulative cycling intensity of the battery system:

$$N_{EFC} = n \times h \tag{6}$$

where N_{EFC} denotes the cumulative number of equivalent full cycles and is dimensionless.

The capacity-loss model can be expressed in terms of the equivalent full cycle number:

$$Q_{\text{loss}}(t) = 30330 \exp\left(\frac{-31500}{8.314T}\right)(2 \times N_{EFC}(t))^{0.552} \tag{7}$$

In the TRNSYS simulation, N_{EFC} is calculated from the cumulative discharged energy:

$$N_{EFC}(t) = N_{EFC}(t-1) + P_{dis,t} \times \Delta t / (\eta_{dis} \times E_{rate}) \tag{8}$$

where $P_{dis,t}$ is the battery discharging power (kW), Δt is the simulation time step (h), η_{dis} is the discharging efficiency, and E_{rate} is the rated battery capacity (kWh).

The battery state of health (SOH) is calculated as:

$$SOH_t = 1 - Q_{\text{loss}}(t) \tag{9}$$

The available battery capacity is calculated as:

$$E_{available,t} = SOH_t \times E_{rate} \quad (10)$$

where E_{rate} is the rated battery energy capacity (kWh).

2.3.2. Limitations of the Battery Aging Model

The adopted degradation model should be interpreted as a simplified system-level cycle-aging model. Cycle aging was estimated from cumulative discharged energy throughput using the Arrhenius-throughput relationship. Calendar aging was not explicitly included in the main simulation. Therefore, the calculated SOH may be optimistic for long-term stationary battery applications, especially when the battery remains at relatively high SOC for long periods.

The model also does not explicitly account for detailed SOC-dependent aging, charge-throughput aging, pack-level cell inconsistency, C-rate variation beyond the fitted C/2 condition, or detailed battery thermal dynamics. Therefore, the calculated SOH should be interpreted as an approximate system-level estimate rather than a precise electrochemical prediction.

The Arrhenius temperature term was evaluated using a constant battery operating temperature of 25 °C, representing a thermally managed battery container or indoor battery room.

2.4. Energy Simulation Models

Transient System Simulation Program (TRNSYS) 18.0 is utilized to conduct simulation studies of the proposed system. Developed by the University of Wisconsin-Madison, TRNSYS is simulation software specifically designed for the analysis of energy systems [46]. Each TRNSYS system consists of interconnected components, and the program's mathematical reference provides equations for each of these components. Figure 2 presents the rooftop PV system of the park, including PV arrays and a battery storage system.

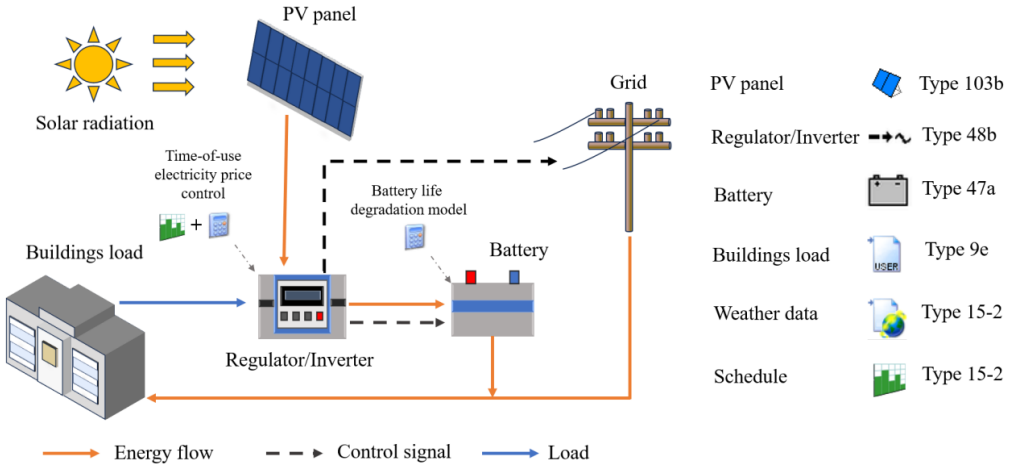

Figure 2. The schematic diagram of the rooftop PV system and the module type.

The components utilized in the simulations are selected from the TRNSYS library, including the TESS library. Type15-3 is used to read the Shanghai weather data downloaded from Meteonorm. Type9e is employed to read the building load calculated in Section 2.2. Type103b and Type47a are applied to simulate the PV module and battery module, respectively. The battery degradation model described in Equations (7)–(10) is incorporated into the simulation. Type14h is used to control the time-of-use electricity pricing signal, and the

output signal is expressed in Equation (11). Type48b is used as the regulator/inverter and is coupled with Type14h and the control equations to manage the system operation.

$$K = \begin{cases} 0, & Peak\ electricity\ price\ time \\ 1, & Off - peak\ electricity\ price\ time \end{cases} \quad (11)$$

The control flowchart is shown in Figure 3. During off-peak electricity-price periods (K = 1), the battery is charged at its maximum allowable power. During peak-price periods (K = 0), the battery is allowed to discharge to meet the building load when ($SOC > SOC_{\min}$). If the PV generation is sufficient to meet the building load ($P_{pv} \geq P_{load}$), the PV electricity is prioritized for supplying the load. When the PV generation exceeds the building load, the surplus PV electricity is used to charge the battery if ($SOC < SOC_{\max}$). If the battery reaches its upper SOC limit, the remaining surplus PV electricity is exported to the grid.

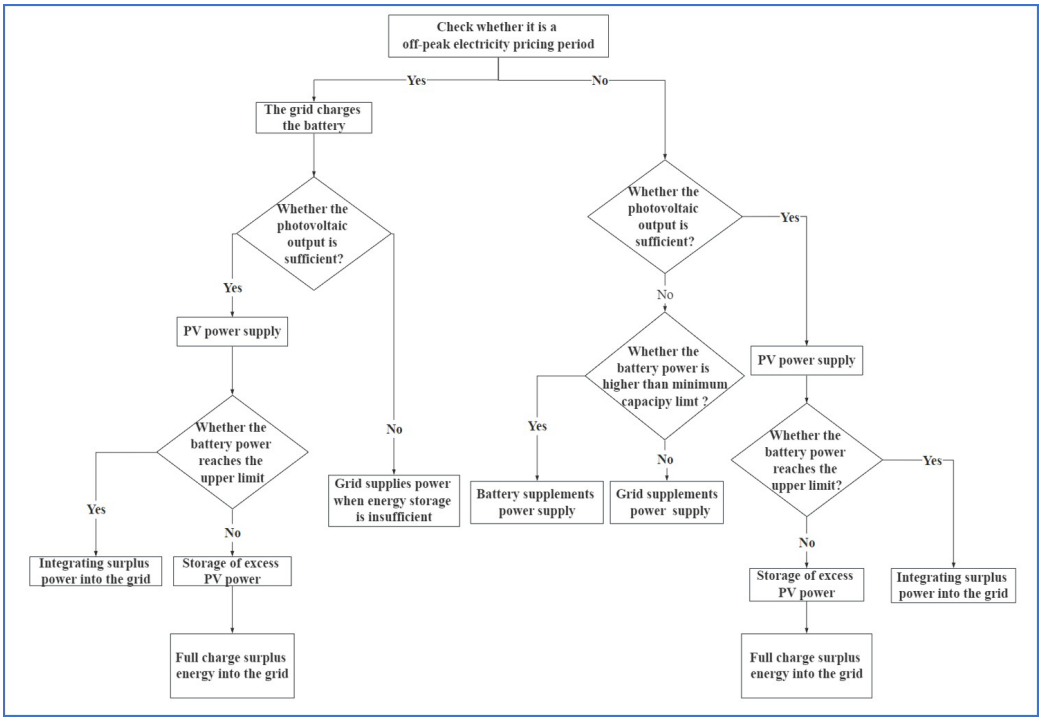

Figure 3. Control flowchart.

To control the battery charge and discharge process, the simulation time step is set to 0.01 h. This time step allows the model to capture the switching behavior when the battery reaches the SOC limits. The PV module degradation is assumed to be 3% initially, followed by an annual degradation rate of 0.7% [47].

2.5. Benefits Assessment

The direct grid supply proportion represents the percentage of building electricity demand directly supplied by the grid. This indicator reflects the degree to which the system depends on grid electricity, in contrast to electricity supplied by rooftop PV or battery storage. The calculation for the direct grid supply proportion is given by Equation (12).

$$D = \frac{E_{grid,load}}{E_{building}} \quad (12)$$

where $E_{grid,load}$ is the building electricity load from the national electricity grid, kWh, $E_{building}$ is the building electricity consumption, kWh.

The CO_2 emission reduction was estimated based on the total PV electricity generation over the project lifetime. The grid emission factor, EF_{grid}, was set as 0.5849 $kgCO_2/kWh$; therefore, the CO_2 emission reduction was calculated using Equation (13).

$$C_{reduction} = E_{pv,total} \times EF_{grid} \tag{13}$$

The net present value approach is employed to evaluate the economic viability of the rooftop system throughout its life cycle. Net present value (NPV) represents the sum of discounted net cash flows over the project evaluation period and is commonly used to assess the economic viability of a project [48]. The calculation for NPV is illustrated in Equation (14). We assume a service life of 25 years for the rooftop PV system.

$$NPV(i) = \sum_{t=0}^{T} F_t(1+i)^{-t} \tag{14}$$

where NPV(i) is the net present value; i is the financial discount rate, which is assumed to be 8% [49]; t is the service time of the PV-battery system; and F_t is the net cash flow, which can be calculated by Equation (15).

$$F_t = CI_t - CO_t \tag{15}$$

where CI is the annual cash inflow, and CO is the annual cash outflow. Their calculations are determined using Equations (16) and (17).

$$CI_t = C_{benefit,t} + C_{dep,battery,t} \tag{16}$$

$$\begin{aligned} CO_t = {} & C_{ivs,battery,t}E_{battery} + C_{ivs,pv,t}P_{pv} + C_{m,pv,t}P_{pv} + C_{r,battery,t}E_{battery} \\ & + C_{r,inverter,t}P_{inverter} \end{aligned} \tag{17}$$

where $C_{ivs,battery,t}$ is the specific investment cost for the energy storage system, CNY/kWh; $C_{ivs,pv,t}$ is the specific investment cost for the rooftop PV system, CNY/kW; $C_{m,pv,t}$ is the maintenance cost of rooftop PV, CNY/kW; and $C_{r,battery,t}$ is the battery replacement cost, assumed to be the battery price in the replacement year. When the available battery capacity falls below 80% of the rated capacity, the battery is retired [50]. Battery costs are expected to decrease in the coming years. The National Renewable Energy Laboratory (NREL) report "Cost Projections for Utility-Scale Battery Storage: 2023 Update" provides battery energy storage cost projections, as shown in Figure 4 [51,52]. The subsequent battery replacement costs were calculated based on the moderate-cost projection scenario. $C_{r,inverter,t}$ is the inverter replacement cost, CNY/kW. $P_{inverter}$ is the inverter power. Following Carlos et al. [53], the inverter replacement costs are defined as 25% of the inverter price in year 5, 45% in year 10, and 60% in years 15 and 20.

$$C_{benefit,t} = C_{pv,t} + C_{battery,t} \tag{18}$$

$$C_{pv,t} = \gamma \times E_{pv,grid,t} + \delta \times \left(E_{pv,user,t} + E_{pv,b,u,t}\right) \tag{19}$$

$$C_{battery,t} = \Delta\delta \times E_{battery,g,u,t} \tag{20}$$

where $C_{benefit,t}$ is the annual income of the system (CNY); $C_{pv,t}$ is the annual income of the PV system (CNY); $C_{battery,t}$ is the annual income of the battery system (CNY); γ is the surplus PV export tariff (CNY/kWh); $E_{pv,grid,t}$ is the PV electricity exported to the grid (kWh); δ is the electricity price (CNY/kWh); $\Delta\delta$ is the difference between peak and off-peak electricity prices (CNY/kWh); $E_{pv,user,t}$ is the PV electricity directly used by the building

load (kWh); $E_{pv,b,u,t}$ is the PV electricity stored in the battery and later supplied to the building load (kWh); and $E_{battery,g,u,t}$ is the grid electricity stored in the battery and later supplied to the building load (kWh). The battery recovery value was calculated using the straight-line depreciation method, assuming a residual value ratio rho of 5% at the end of the battery lifespan.

$$C_{dep,battery,t} = E_{battery} C_{battery,new,t} [\rho + (1 - \rho) \times \frac{L - N}{L}] \quad (21)$$

where $C_{dep,battery,t}$ is the battery recovery value (CNY); $C_{battery,new,t}$ is the battery replacement price in year t (CNY/kWh); L is the battery lifespan (year); and N is the battery usage time before recycling (year).

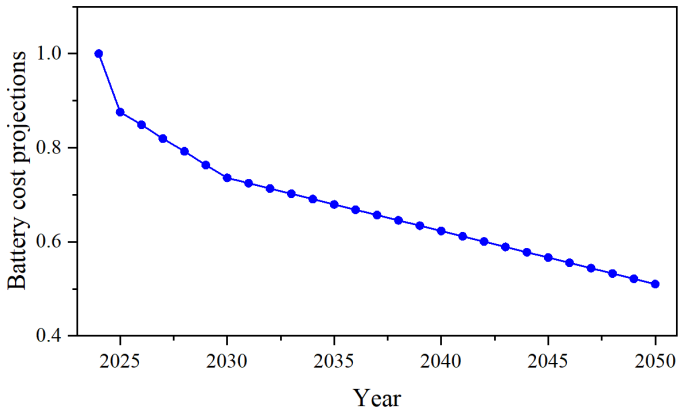

Figure 4. Battery cost projections with value normalized relative to 2024.

$C_{battery,new,t}$ was calculated as:

$$C_{battery,new,t} = C_{ivs,battery,0} \times C_{NREL,t} / C_{NREL,0} \quad (22)$$

where $C_{NREL,t}$ is the projected NREL battery costs in year t and the base year, respectively. Their ratio represents the normalized battery-cost proportion relative to the base year. Therefore, currency conversion was not required because only the relative cost-reduction trend was applied.

3. Case Study and Simulation Settings

3.1. Study Area and Building Load Modeling

The case study was conducted for an urban industrial park in Shanghai, China. The park is located at approximately 31.2° N and 121.6° E (Figure 5), and its building stock consists mainly of office buildings, with additional commercial, school, and residential buildings. The total building footprint extracted from the GIS data was 230,660 m^2, including 171,236 m^2 of office buildings, 20,777 m^2 of commercial buildings, 6877 m^2 of school buildings, and 31,770 m^2 of residential buildings.

Due to the lack of measured electricity data for each individual building in the park, representative EnergyPlus models were used to generate hourly electricity demand profiles for each building type. The internal load parameters, including lighting and plug/equipment power densities, were assigned according to the relevant Chinese building energy-efficiency design standards for civil and public buildings [54]. The EnergyPlus models included lighting and plug/equipment electricity consumption, while heating-related electricity demand from heat pumps or electric heaters was not included.



Figure 5. Study area.

The main internal load settings used in the EnergyPlus models are summarized in Table 2. The simulated hourly profiles were scaled according to the corresponding building floor areas and then aggregated to obtain the park-level hourly electricity demand used as the load input in TRNSYS.

Table 2. Building load modeling settings used in EnergyPlus.

Building Type	Floor Area Used for Load Aggregation (m^2)	Lighting Power Density (W/m^2)	Equipment Power Density (W/m^2)
Office	1,651,417	8	15
Commercial	123,728	9	13
School buildings	104,571	8	5
Residential	459,354	5	3.8

3.2. System Specification and Simulation Settings

The main PV-battery system specifications and TRNSYS simulation settings are summarized in Table 3.

The PV output of the whole park was calculated by scaling the output of a single PV module according to the usable rooftop area. The usable rooftop area obtained from the GIS-based rooftop suitability assessment was 113,208 m^2. The PV module area was 1.75 m^2, and the module rated power was approximately 290.07 Wp, calculated from the voltage and current at the maximum power point. Therefore, the total number of installable modules was 64,690, corresponding to a total installed PV capacity of approximately 18,765 kWp. The installed capacity refers to the rated peak capacity under standard test conditions.

Type103b calculates PV output using ambient temperature and incident radiation on the tilted surface, with the reference cell temperature and NOCT set to 24.85 °C and 45.35 °C, respectively. The battery charging efficiency was set to 0.90, while no separate discharge-loss parameter was specified in Type47a; therefore, the discharging efficiency was treated as 1.00. The maximum battery charging and discharging powers were both limited to 0.5C. Therefore, for the evaluated battery capacities ranging from 5000 to 40,000 kWh, the corresponding maximum charging and discharging powers ranged from 2500 to 20,000 kW.

Table 3. System specifications and TRNSYS simulation settings.

Category	Parameter	Value/Assumption
PV system	TRNSYS model	Type103b with MPPT
PV system	Module rated power	290.07 Wp
PV system	Module area	1.75 m^2
PV system	Total installed capacity	18,765 kWp
PV system	PV degradation	3% initial degradation and 0.7% annual degradation
PV system	Array tilt angle	24°
PV system	Array azimuth angle	0°
PV system	Reference cell temperature	24.85 °C
PV system	Nominal operating cell temperature	45.35 °C
Inverter/regulator	TRNSYS model	Type48b
Inverter/regulator	Regulator efficiency	0.95
Inverter/regulator	Inverter efficiency	1.00
Battery system	TRNSYS battery model	Type47a
Battery system	Battery chemistry	$LiFePO_4$
Battery system	Candidate battery capacity	5000–40,000 kWh
Battery system	Maximum charging and discharging power	0.5C, corresponding to 2500–20,000 kW
Battery system	Charging efficiency	0.90
Battery system	Initial SOC	0.20
Battery system	SOC range	0.10–0.90
Battery system	End-of-life criterion	SOH $\leq$ 0.80
Grid/export	Export limit	No explicit export power limit was imposed
Simulation	Weather file	Meteonorm-generated TMY2 weather file for Shanghai
Simulation	Time step	0.01 h

The candidate battery capacity ranged from 5000 to 40,000 kWh. The SOC was limited to 0.10–0.90 to avoid over-charge and deep discharge, and the battery end of life was defined as SOH $\leq$ 0.80. The simulation used a Meteonorm-generated TMY2 weather file for Shanghai and a time step of 0.01 h [55].

3.3. Economic Assessment Settings

The main economic and policy parameters used in the NPV assessment are summarized in Table 4. The project lifetime of the rooftop PV system was assumed to be 25 years, and the discount rate was set to 8%. The electricity price was modeled as a time-of-use tariff according to the peak and off-peak electricity prices in Shanghai.

Table 4. Input parameters for economic assessment.

	Specific Costs
Battery cost	1100 CNY/kWh
PV cost	3600 CNY/kW
Inverter cost	460 CNY/kW
PV maintenance cost	48 CNY/kW
Surplus PV export tariff	0.4155 CNY/kWh
Electricity price of Shanghai city (time-of-use tariff)	6:00–22:00: 0.9581 CNY/kWh 22:00–6:00: 0.4997 CNY/kWh

4. Results and Discussion

4.1. Suitable Area Calculation and PV Power Generation

Figure 6 presents the GIS-based rooftop suitability assessment for the park. Based on the building footprints and the rooftop usable-area reduction coefficients in Table 1, the final usable rooftop area for PV installation was calculated as 113,208 m^2.

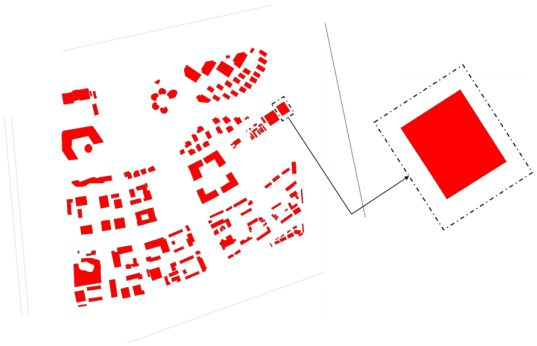

Figure 6. Calculation of the useful area in the park buildings.

Figure 7 presents the annual solar irradiance obtained from the Meteonorm-generated weather file for Shanghai. The maximum solar irradiance reaches 1000.8 W/m^2. Figure 8 presents the annual PV power output. Based on the PV system specifications described in Section 3.2, the annual rooftop PV generation is approximately 24.7 GWh, corresponding to a specific PV yield of approximately 1316 kWh/(kWp·yr). The annual electricity consumption of the park is approximately 100.2 GWh, corresponding to an electricity use intensity of approximately 42.84 kWh/(m^2·yr). Therefore, the rooftop PV system supplies approximately 24.7% of the annual electricity demand on an energy basis rather than on a peak-power basis. After accounting for PV degradation, the cumulative PV generation over the 25-year project lifetime is approximately 574.4 GWh.

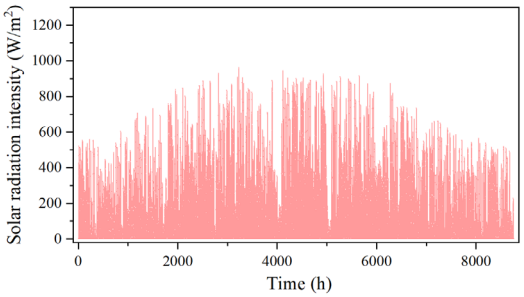

Figure 7. Solar radiation intensity of the Shanghai area.

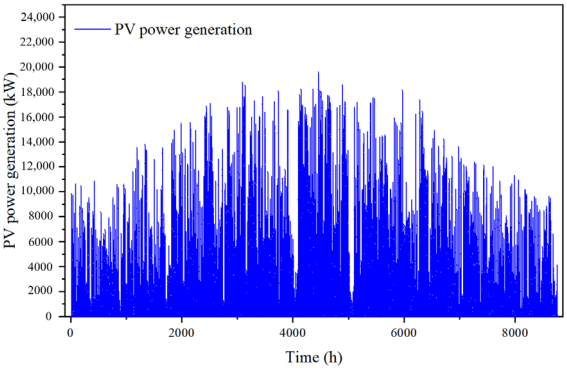

Figure 8. PV power generation.

4.2. Time-Step Sensitivity Analysis

A time-step sensitivity analysis was conducted to confirm the numerical robustness of the simulation. Three time steps, 0.01 h, 0.05 h, and 0.10 h, were compared using the same weather data, load profile, PV capacity, battery parameters, and control logic. The final battery SOH after one year of operation was used as the main indicator for evaluating the influence of the time step on the degradation calculation.

The comparison showed that the battery degradation result was only slightly affected by the simulation time step. The final battery SOH values were 96.76%, 96.74%, and 96.71% for time steps of 0.01 h, 0.05 h, and 0.10 h, respectively. The maximum difference among the three cases was only 0.05 percentage points. This indicates that the degradation result was not sensitive to the selected time step. Therefore, the 0.01 h time step was computationally feasible and was retained in the main simulation to better capture the charge–discharge switching behavior of the battery and reduce numerical errors in SOC control.

4.3. Model Validation

To validate the battery degradation model used in this study, a literature-based validation was conducted using the experimental graphite-$LiFePO_4$ cycle-life data reported by Wang et al. [45]. The measured capacity-loss data at 15 degrees C under the C/2 discharge-rate condition were digitized from the published experimental figure.

Figure 9 compares the experimental data with the model simulation results. The model reproduces the experimental trend well. The capacity loss increases with cumulative equivalent full cycles, and the simulated curve is close to the measured values over the tested range. This indicates that the adopted degradation equation can reasonably represent the cycle-aging behavior of graphite-$LiFePO_4$ cells under low-rate cycling conditions.

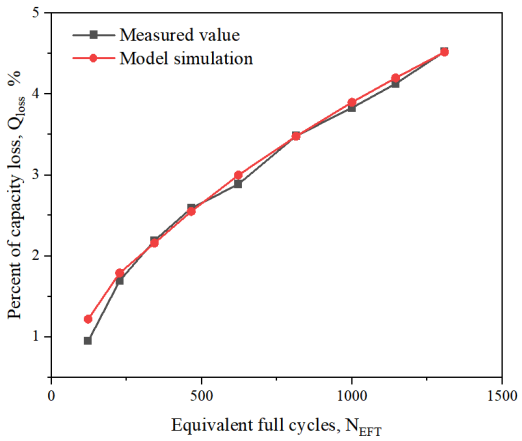

Figure 9. Validation of the battery degradation model against experimental data.

4.4. Example-Day Operation and Control Behavior

Figure 10 illustrates an example of the battery SOC within the energy system corresponding to a battery capacity of 10,000 kWh. The example day is a weekend, and the building load is 42,808 kWh. From 0:00 to 2:27, the battery SOC increases from 0.46 to 0.90 because the system is in the off-peak period and the battery is charged at its maximum power. Subsequently, the SOC remains at 0.90 until 6:00 because the upper SOC limit is reached. From 6:00 to 8:03, the SOC decreases from 0.90 to 0.54 as the battery begins to supply energy to the buildings during the peak electricity period. The SOC then increases from 0.54 to 0.90 between 8:03 and 8:56 because PV generation exceeds the building load and the surplus PV electricity charges the battery. Due to the battery charging protection mechanism, the SOC remains at 0.90 until 16:13. When PV generation becomes lower than

the building load, the battery discharges from 0.90 to 0.10 between 16:13 and 19:18. At 22:00, when the off-peak period starts, the battery begins charging again.

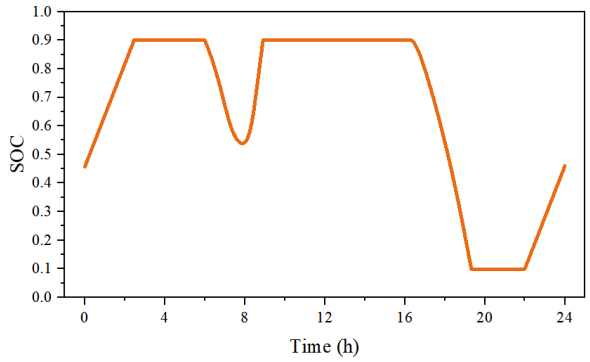

Figure 10. Battery SOC changes for an example day with a battery capacity of 10,000 kWh.

Figure 11 shows the energy flows corresponding to the battery capacity of 10,000 kWh on the same day. Negative grid-export values indicate that PV electricity or battery electricity is fed back to the grid. The battery discharge curve is consistent with the SOC variation. The grid supplies electricity to both the battery and the buildings between 0:00 and 2:27. After the battery is fully charged, the grid supplies only the building load. Between 8:56 and 16:13, PV generation is higher than the building load, and the battery is fully charged; therefore, excess PV electricity is exported to the grid. At 19:18, the battery reaches the lower SOC limit, and the grid begins to supply the building load. Finally, as the off-peak period arrives, the grid begins to charge the battery. On this day, the total PV generation is 67,465 kWh. Approximately 40,973 kWh is exported to the grid, 4027 kWh charges the battery, and 19,091 kWh is supplied directly to the buildings. The grid supplies about 21,020 kWh, including 12,153 kWh to the buildings and 8940 kWh to the battery. The battery discharging and charging energy are approximately 11,637 kWh and 12,967 kWh, respectively.

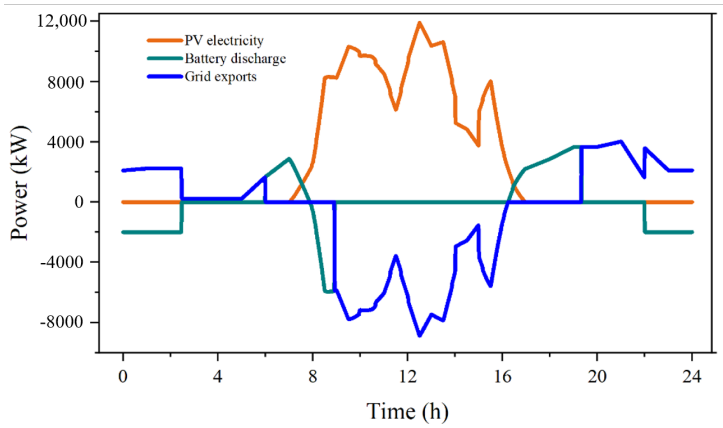

Figure 11. Energy flows for an example day with a battery capacity of 10,000 kWh.

4.5. Effect of Battery Capacity on System Operation

Figure 12 shows the effect of battery capacity on the annual battery electricity supplied to the building load and the direct grid supply proportion. As the battery capacity increases from 5000 kWh to 40,000 kWh, the annual battery electricity supplied to the load increases from 2.16 GWh to 13.39 GWh. This indicates that a larger battery can provide stronger load-shifting capability.

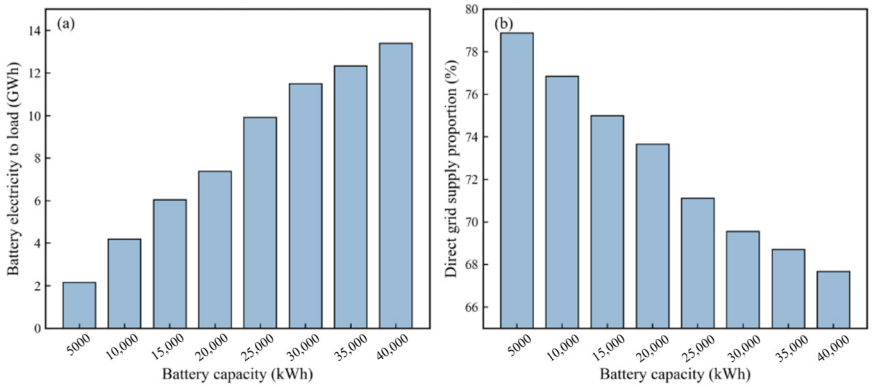

Figure 12. The effect of battery capacity on (**a**) battery electricity supplied to the building load and (**b**) direct grid supply proportion.

Meanwhile, the proportion of electricity supplied directly from the grid to the building load decreases from 78.88% at 5000 kWh to 67.67% at 40,000 kWh. This trend indicates that increasing battery capacity can reduce the direct dependence of the building load on grid electricity. However, the reduction becomes more gradual at larger capacities, suggesting that the operational benefit of additional battery capacity gradually approaches saturation.

Therefore, increasing battery capacity can improve the operational performance of the PV-battery system by increasing battery discharge to the load and reducing direct grid supply. However, larger battery capacities also lead to higher investment costs and potential replacement costs, which are further evaluated through the NPV analysis.

For the recommended 30,000 kWh configuration, additional operational indicators were calculated to provide a more comprehensive assessment of system operation. The PV self-consumption ratio was 79.93%, indicating that most of the annual PV generation was directly consumed by the building or used to charge the battery. The locally utilized PV electricity corresponded to approximately 20.29% of the annual building electricity demand. Because grid charging was permitted under the adopted control strategy, the total battery electricity supplied to the building load was not treated as renewable self-supply. The annual battery discharge throughput was approximately 11.50 GWh, corresponding to 383.26 equivalent full cycles per year.

4.6. Battery Degradation Under Different Capacities

Figure 13 illustrates the final SOH of the battery after one year of operation (8760 h) under different battery capacities. When the battery capacity increases from 5000 kWh to 40,000 kWh, the final SOH increases from 96.16% to 96.67%. This indicates that the annual battery degradation decreases as the battery capacity increases, although the improvement becomes more gradual at larger capacities. This trend is mainly because, under the same load profile and control strategy, a larger battery experiences lower equivalent cycling intensity and a smaller relative depth of discharge. Therefore, increasing the battery capacity can reduce the annual degradation rate of the battery.

4.7. Economic Performance and Recommended Battery Capacity

In this study, the recommended battery capacity was determined using a parametric techno-economic sizing approach. Candidate battery capacities ranging from 5000 to 40,000 kWh were simulated under the same PV capacity, load profile, tariff structure, control strategy, and battery degradation model. Under the baseline operating condition, the maximum battery charging and discharging rates were both limited to 0.5C. The capacity producing the maximum NPV was selected as the recommended battery capacity.

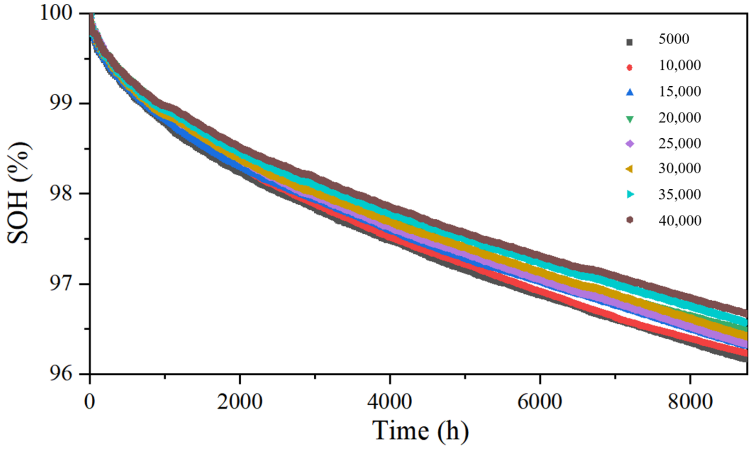

Figure 13. The SOH of different battery capacities.

Figure 14 shows the NPV results under different battery capacities. The NPV initially increases with battery capacity because a larger battery increases the amount of electricity shifted from off-peak to peak-price periods and reduces direct grid electricity supply to the building load. However, the marginal operational benefit gradually decreases as battery capacity increases, while the investment and replacement costs continue to increase. Consequently, the NPV decreases after reaching its maximum value.

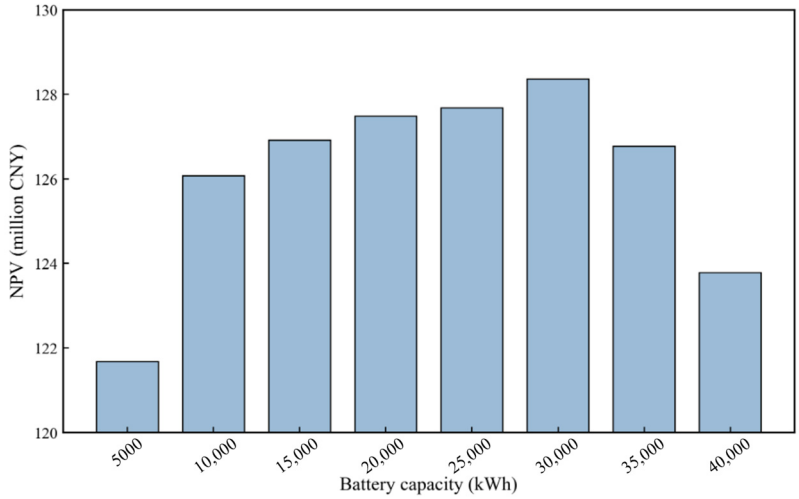

Figure 14. The effect of battery capacity on NPV under the constrained 0.5C grid-charging strategy.

Under the baseline 0.5C condition, the maximum NPV is obtained at a battery capacity of 30,000 kWh, with an NPV of 128.36 million CNY. The simple and discounted payback periods of this configuration are approximately 4.6 and 6.0 years, respectively. Therefore, 30,000 kWh is selected as the recommended battery capacity under the baseline operating condition.

To evaluate the robustness of the recommended capacity against changes in battery operating constraints, an additional targeted sensitivity test was conducted by reducing both the maximum battery charging and discharging rates from 0.5C to 0.2C. All other technical, economic, and control parameters were maintained unchanged. Under the constrained 0.2C condition, the maximum NPV was obtained at a battery capacity of 35,000 kWh, as shown in Figure 15. However, the NPV of the 30,000 kWh configuration was only approximately 1.14% lower than the maximum value. These results indicate that the precise economic optimum is moderately affected by the charge–discharge-rate constraint, while the economically favorable capacity range remains between 30,000 and 35,000 kWh.

Therefore, the baseline recommendation of 30,000 kWh remains a robust and comparatively conservative configuration.

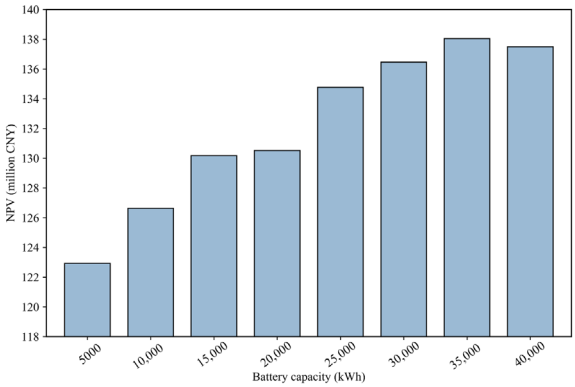

Figure 15. Effect of battery capacity on NPV under the constrained 0.2C grid-charging strategy.

Over the 25-year project lifetime, the rooftop PV system generates approximately 574.4 GWh of electricity after considering PV degradation, corresponding to a CO_2 emission reduction of approximately 335,967 tCO_2. The recommended battery capacity should therefore be interpreted as the economic optimum under the specified operating conditions, whereas the CO_2 emission reduction is mainly determined by rooftop PV generation.

4.8. Sensitivity Analysis

4.8.1. Effect of BES Cost on Recommended Battery Capacity

The sensitivity of the recommended battery capacity to BES cost was analyzed by varying the BES cost from 800 to 1300 CNY/kWh. As shown in Figure 16, BES cost has a significant influence on both the maximum NPV and the recommended battery capacity. When the BES cost is between 800 and 1100 CNY/kWh, the optimal battery capacity remains 30,000 kWh, and the maximum NPV decreases from 137.82 million CNY to 128.36 million CNY as the BES cost increases. When the BES cost further increases to 1200 CNY/kWh and 1300 CNY/kWh, the recommended battery capacity decreases to 20,000 kWh and 10,000 kWh, respectively. This indicates that large-capacity battery configurations are economically attractive only when the BES investment cost is sufficiently low. As the BES cost increases, the additional revenue obtained from larger battery capacities can no longer offset the higher initial investment and replacement costs. Therefore, BES cost is one of the key factors affecting the techno-economic sizing of rooftop PV-battery systems in industrial parks.

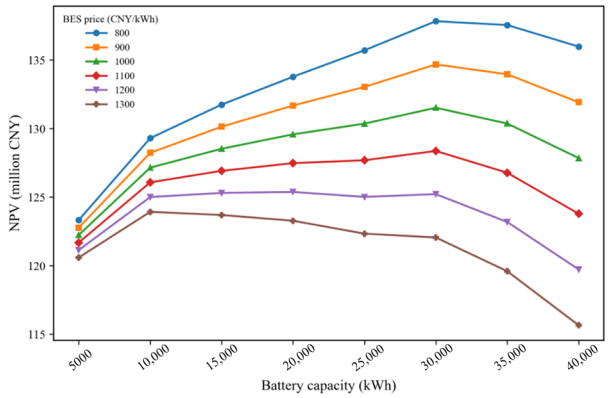

Figure 16. Sensitivity of NPV and recommended battery capacity to BES cost.

4.8.2. Effect of Tariff Spread on Recommended Battery Capacity

The sensitivity of the recommended battery capacity to the tariff spread was analyzed by varying the peak-off-peak electricity price difference from 0.30 to 0.60 CNY/kWh. The results are shown in Figure 17. When the tariff spread is relatively low, at 0.30 and 0.40 CNY/kWh, the optimal battery capacity is 10,000 kWh, with maximum NPVs of 120.08 million CNY and 123.86 million CNY, respectively. This is because a small tariff spread provides limited economic benefit for load shifting, and the additional investment cost of a larger battery cannot be offset by the increased arbitrage revenue.

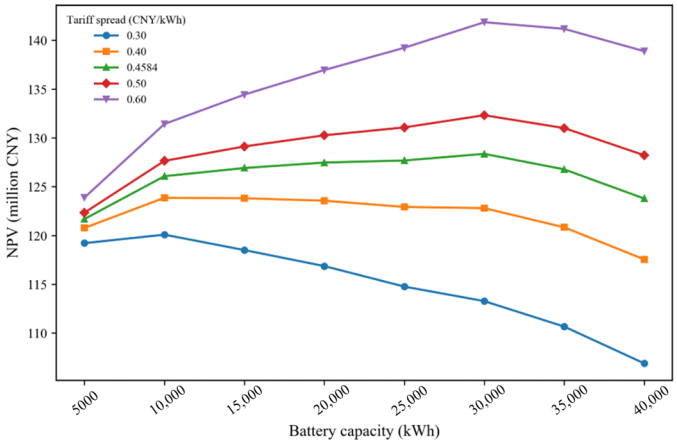

Figure 17. Effect of tariff spread on NPV under different battery capacities.

Under the current Shanghai tariff spread of 0.4584 CNY/kWh, the recommended battery capacity increases to 30,000 kWh, with a maximum NPV of 128.36 million CNY. When the tariff spread further increases to 0.50 and 0.60 CNY/kWh, the optimal capacity remains 30,000 kWh, while the maximum NPV increases to 132.32 million CNY and 141.85 million CNY, respectively. This indicates that a larger peak-off-peak tariff spread improves the economic value of battery storage by increasing the benefit of charging during off-peak periods and discharging during peak periods. Therefore, the tariff spread is a key policy-related factor affecting the techno-economic sizing of PV-battery systems in industrial parks.

4.8.3. Effect of Discount Rate on Recommended Battery Capacity

The sensitivity of the recommended battery capacity to the discount rate was analyzed by varying the discount rate from 4% to 12%. The results are shown in Figure 18. When the discount rates are 4%, 6%, and 8%, the optimal battery capacity remains 30,000 kWh, with maximum NPVs of 230.50 million CNY, 172.12 million CNY, and 128.36 million CNY, respectively. This indicates that the 30,000 kWh configuration remains economically favorable under low-to-moderate discount-rate assumptions.

However, when the discount rate increases to 10% and 12%, the recommended battery capacity decreases to 15,000 kWh and 10,000 kWh, respectively. This is because a higher discount rate reduces the present value of future electricity savings and long-term operational benefits, while the initial investment cost of the battery system is paid at the beginning of the project. As a result, larger battery capacities become less economically attractive under higher discount-rate conditions. Therefore, the discount rate is an important financial parameter affecting the techno-economic sizing of PV-battery systems.

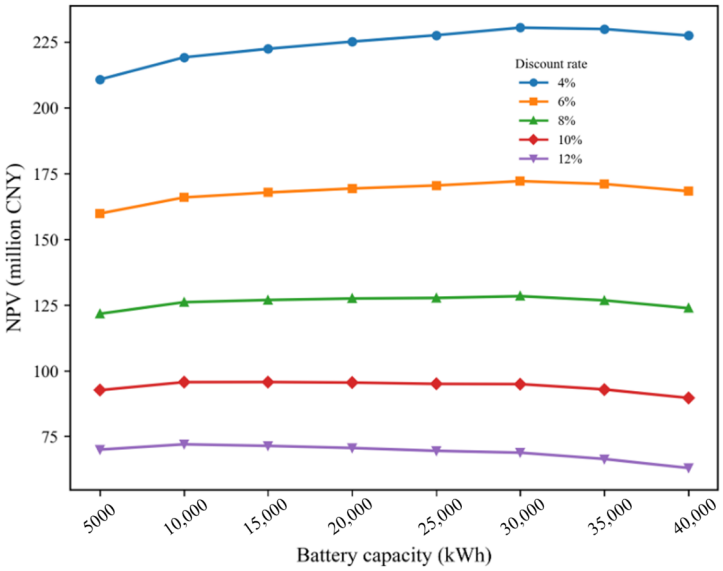

Figure 18. Effect of discount rate on NPV under different battery capacities.

4.8.4. Effect of Export Price on Recommended Battery Capacity

The sensitivity of the recommended battery capacity to the PV export price was analyzed by varying the export price from 0.20 to 0.60 CNY/kWh. The results are shown in Figure 19. As the export price increases, the NPV of all battery capacity configurations increases because the revenue from surplus PV electricity exported to the grid becomes higher.

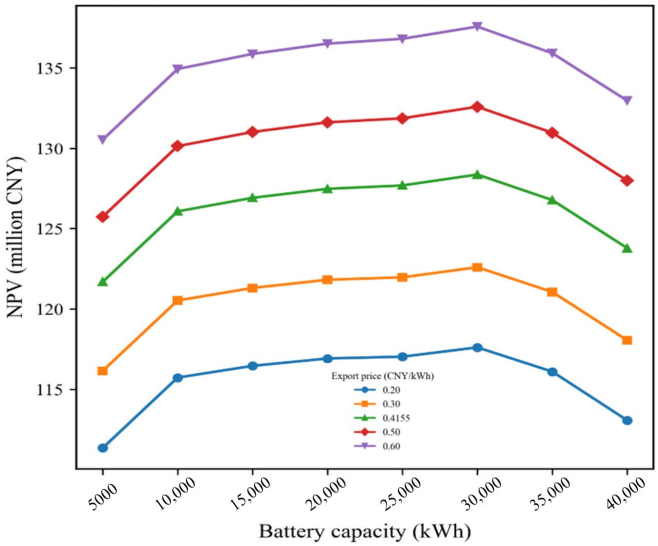

Figure 19. Effect of export price on NPV under different battery capacities.

When the export price increases from 0.20 to 0.60 CNY/kWh, the maximum NPV increases from 117.60 million CNY to 137.57 million CNY. This change is mainly caused by the relatively large amount of PV electricity exported to the grid. For example, in the 30,000 kWh case, the annual PV electricity exported to the grid is approximately 5.10 GWh. Therefore, an increase of 0.10 CNY/kWh in the export price can increase the annual export revenue by approximately 0.51 million CNY before discounting. Over the 25-year project period, this leads to a noticeable change in NPV.

However, the recommended battery capacity remains 30,000 kWh under all tested export-price scenarios. This indicates that although the export price has a clear influence on the overall project profitability, it has a limited effect on the recommended battery capacity

in this case. The reason is that the export-price change mainly affects the PV export revenue, while the battery sizing is more strongly influenced by the load-shifting benefit, BES cost, and replacement cost. Therefore, the 30,000 kWh configuration is relatively robust with respect to the PV export price.

4.8.5. Effect of Battery Degradation Coefficient on Recommended Battery Capacity

The sensitivity of the recommended battery capacity to the battery degradation coefficient was analyzed by multiplying the baseline degradation coefficient by 0.8 and 1.2, while keeping the PV capacity, load profile, BES cost, tariff structure, SOH replacement threshold, and control strategy unchanged. The baseline case was represented by a multiplier of 1.0. The results are shown in Figure 20.

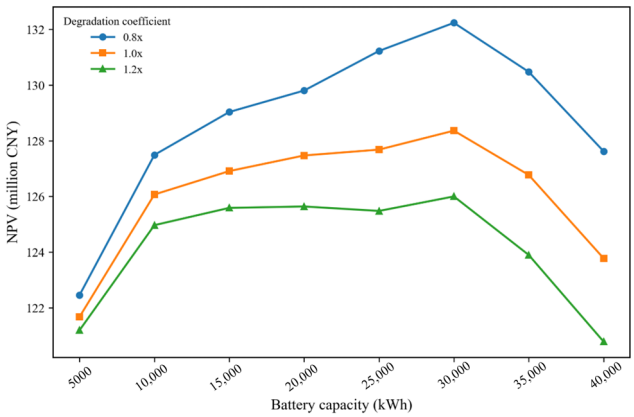

Figure 20. Effect of battery degradation coefficient on NPV under different battery capacities.

When the degradation coefficient is reduced to 0.8 times the baseline value, the maximum NPV increases to 132.23 million CNY, while the optimal battery capacity remains 30,000 kWh. This is because a lower degradation rate slows down the SOH decline and delays battery replacement, thereby reducing the discounted replacement cost over the project lifetime. When the degradation coefficient is increased to 1.2 times the baseline value, the maximum NPV decreases to 126.00 million CNY. Although the NPV changes with the degradation coefficient, the recommended battery capacity remains 30,000 kWh under all tested degradation scenarios. This indicates that the recommended capacity is relatively robust to moderate uncertainty in the degradation coefficient.

5. Conclusions

This paper proposes a techno-economic sizing method for rooftop PV-battery systems in urban industrial parks, taking battery life degradation into account. NPV is used as the main economic evaluation metric. A case study is conducted in an urban industrial park in Shanghai, China, to demonstrate the applicability of the method. The operational performance, battery degradation behavior, economic performance, carbon emission reduction, and parameter sensitivities are analyzed. The main conclusions are as follows.

(1) The TRNSYS-based PV-battery model coupled with user-defined degradation equations can capture the interaction among PV generation, building load, battery operation, SOC constraints, and degradation-aware capacity updates. This indicates that the proposed modeling framework is suitable for evaluating long-term PV-battery operation in industrial parks where battery cycling behavior and replacement timing are closely linked to system economics.

(2) Rooftop PV alone can provide a considerable but limited contribution to the park's electricity demand. The usable rooftop area was estimated as 113,208 m^2, corresponding

to an installed PV capacity of approximately 18,765 kWp. The annual PV generation was approximately 24.7 GWh, accounting for 24.7% of the annual electricity demand. This shows that rooftop PV can reduce grid dependence, but battery storage is still needed to improve local utilization and load-shifting performance.

(3) Increasing battery capacity improves load shifting, but the operational benefit shows clear saturation. When battery capacity increases from 5000 kWh to 40,000 kWh, the annual electricity supplied from the battery to the building load increases from 2.16 GWh to 13.39 GWh, while the direct grid supply proportion decreases from 78.88% to 67.67%. However, the reduction in grid dependence becomes progressively smaller at larger capacities, indicating that oversizing the battery provides limited additional operational benefit.

(4) Battery degradation is strongly affected by capacity sizing. Larger battery capacities reduce the equivalent cycling intensity and slow down annual SOH decline. The final SOH after one year increases from 96.16% at 5000 kWh to 96.67% at 40,000 kWh. This result indicates that battery capacity sizing affects not only short-term energy dispatch but also long-term degradation and replacement cost, which should not be ignored in techno-economic assessment.

(5) The economically optimal battery capacity is not the largest capacity but the capacity that balances load-shifting benefit, degradation mitigation, investment cost, and replacement cost. In the studied park, the maximum NPV is obtained at 30,000 kWh, with an NPV of 128.36 million CNY. The simple payback period is approximately 4.6 years, and the discounted payback period is approximately 6.0 years. This indicates that increasing battery capacity beyond 30,000 kWh leads to insufficient additional revenue to offset the higher capital and replacement costs.

(6) The sensitivity analysis shows that battery sizing is most affected by BES cost, tariff spread, and discount rate. Lower BES cost and larger peak-off-peak tariff spread support larger battery capacity, while higher discount rates favor smaller capacity because future operational savings are discounted more strongly. By contrast, PV export price mainly changes the overall NPV but has limited influence on the recommended battery capacity. This suggests that battery investment cost and time-of-use tariff design are the key policy and market factors determining the economic feasibility of large-scale battery deployment in industrial parks.

These conclusions provide useful methodological references for integrating rooftop PV-battery systems into large-scale energy-saving renovation projects in urban industrial parks. However, the present study still has several limitations. The adopted battery degradation model is a simplified system-level cycle-aging model that mainly considers cumulative cycling intensity, depth of discharge, and the Arrhenius temperature effect. Calendar aging, SOC-window-dependent degradation, C-rate variation, charging behavior, thermal gradients, and dynamic battery temperature variations were not explicitly modeled. Therefore, the calculated SOH should be interpreted as an approximate degradation indicator, and the model may underestimate battery degradation when batteries remain at high SOC for long periods.

In addition, the economic assessment was based on the time-of-use electricity price and policy assumptions in Shanghai. The economic performance may vary with different electricity pricing policies, PV export tariffs, battery prices, PV investment costs, discount rates, and load profiles. Although one-at-a-time sensitivity analyses were conducted for several key parameters, a full probabilistic uncertainty analysis was not performed in this study. Therefore, the robustness of the recommended battery capacity under stochastic solar radiation, load uncertainty, and long-term market uncertainty should be further investigated. Moreover, comparison across other climates, battery technologies, and advanced

operating strategies remains valuable and should be further explored in future studies by taking advantage of the modularity and flexibility of TRNSYS.

Author Contributions: Methodology, Y.X.; Software, Y.X.; Validation, Y.X.; Formal analysis, T.S. and Q.H.; Investigation, H.Z.; Data curation, Y.X.; Writing—original draft, Y.X.; Writing—review & editing, Y.X.; Visualization, Y.X.; Supervision, H.Z.; Project administration, Z.L. and H.Z.; Funding acquisition, Z.L. and H.Z. All authors have read and agreed to the published version of the manuscript.

Funding: This study was supported by the National Natural Science Foundation of China (Grant No. 52478102).

Data Availability Statement: The original contributions presented in the study are included in the article, further inquiries can be directed to the corresponding author.

Acknowledgments: The authors acknowledge the support provided during the preparation of this manuscript.

Conflicts of Interest: The authors declare no conflict of interest.

References

1. Nematchoua, M.K.; Yvon, A.; Roy, S.E.J.; Ralijaona, C.G.; Mamiharijaona, R.; Razafinjaka, J.N.; Tefy, R. A review on energy consumption in the residential and commercial buildings located in tropical regions of Indian Ocean: A case of Madagascar island. *J. Energy Storage* **2019**, *24*, 100748. [CrossRef]
2. Nematchoua, M.K.; Nishimwe, M.R.; Reiter, S. Towards nearly zero-energy residential neighbourhoods in the European Union: A case study. *Renew. Sustain. Energy Rev.* **2021**, *135*, 110198. [CrossRef]
3. Wei, Y.-M.; Chen, K.; Kang, J.-N.; Chen, W.; Wang, X.-Y.; Zhang, X. Policy and management of carbon peaking and carbon neutrality: A literature review. *Engineering* **2022**, *14*, 52–63. [CrossRef]
4. Wang, S.; Zhenghong, J. Research on the decoupling relationship between carbon emission and economic growth under dual carbon policy:based on the empirical evidence of prefecture-level cities in Anhui, Jiangsu and Zhejiang Provinces. *Coal Econ. Res. Coal Econ. Res.* **2022**, *42*, 4–12.
5. Bin, C.; Guoxuan, H.; Jing, Q.; Meirong, S.; Shiyi, Z.; Meiming, J. Greenhouse Gas Inventory of a Typical High-End Industrial Park in China. *Sci. World J.* **2013**, *2013*, 717054. [CrossRef]
6. Jing, Y.; Zhu, L.; Yin, B.; Li, F. Evaluating the PV system expansion potential of existing integrated energy parks: A case study in North China. *Appl. Energy* **2023**, *330*, 120310. [CrossRef]
7. Guo, Y.; Tian, J.; Chen, L. Managing energy infrastructure to decarbonize industrial parks in China. *Nat. Commun.* **2020**, *11*, 981. [CrossRef] [PubMed]
8. Li, M.; Gao, Y.; Meng, B.; Yang, Z. Managing the mitigation: Analysis of the effectiveness of target-based policies on China's provincial carbon emission and transfer. *Energy Policy* **2021**, *151*, 112189. [CrossRef]
9. Lalwani, M.; Kothari, D.P.; Singh, M. Viability analysis by techno-economic aspects of grid interactive solar photovoltaic project in india. In Proceedings of the IEEE-International Conference on Advances in Engineering, Science And Management (ICAESM-2012), Nagapattinam, India, 30–31 March 2012.
10. Zahedi, A. Solar photovoltaic (PV) energy; latest developments in the building integrated and hybrid PV systems. *Renew. Energy* **2006**, *31*, 711–718. [CrossRef]
11. Hegedus, S.S.; Luque, A. Status, Trends, Challenges and the Bright Future of Solar Electricity from Photovoltaics. In *Handbook of Photovoltaic Science and Engineering*; John Wiley & Sons: Hoboken, NJ, USA, 2005.
12. He, L.; Li, C.L.; Nie, Q.Y.; Men, Y.; Zhu, J. Core Abilities Evaluation Index System Exploration and Empirical Study on Distributed PV-Generation Projects. *Energies* **2017**, *10*, 2083. [CrossRef]
13. Wang, P.; Yu, P.; Huang, L.; Zhang, Y. An integrated technical, economic, and environmental framework for evaluating the rooftop photovoltaic potential of old residential buildings. *J. Environ. Manag.* **2022**, *317*, 115296. [CrossRef]
14. Duman, A.C.; Güler, Ö. Economic analysis of grid-connected residential rooftop PV systems in Turkey. *Renew. Energy* **2020**, *148*, 697–711. [CrossRef]
15. Lee, J.; Chang, B.; Aktas, C.; Gorthala, R. Economic feasibility of campus-wide photovoltaic systems in New England. *Renew. Energy* **2016**, *99*, 452–464. [CrossRef]
16. Gomez-Exposito, A.; Arcos-Vargas, A.; Gutierrez-Garcia, F. On the potential contribution of rooftop PV to a sustainable electricity mix: The case of Spain. *arXiv* **2020**, arXiv:2005.10911.

17. Miao, R.; Zhu, H.; Zhang, Y.; Li, K.; Yuan, Y.; Shen, P.; Qi, H. Rooftop PV layout generation and optimization model for large-scale building cluster. *Sustain. Cities Soc.* **2026**, *137*, 107129. [CrossRef]
18. Luthander, R.; Widen, J.; Nilsson, D.; Palm, J. Photovoltaic self-consumption in buildings: A review. *Appl. Energy* **2015**, *142*, 80–94. [CrossRef]
19. Ziegler, M.S.; Trancik, J.E. Re-examining rates of lithium-ion battery technology improvement and cost decline. *Energy Environ. Sci.* **2021**, *14*, 1635–1651. [CrossRef]
20. Stephan, A.; Battke, B.; Beuse, M.D.; Clausdeinken, J.H.; Schmidt, T.S. Limiting the public cost of stationary battery deployment by combining applications. *Nat. Energy* **2016**, *1*, 16079. [CrossRef]
21. Han, X.; Garrison, J.; Hug, G. Techno-economic analysis of PV-battery systems in Switzerland. *Renew. Sustain. Energy Rev.* **2022**, *158*, 112028. [CrossRef]
22. Schopfer, S.; Tiefenbeck, V.; Staake, T. Economic assessment of photovoltaic battery systems based on household load profiles. *Appl. Energy* **2018**, *223*, 229–248. [CrossRef]
23. Tervo, E.; Agbim, K.; DeAngelis, F.; Hernandez, J.; Kim, H.K.; Odukomaiya, A. An economic analysis of residential photovoltaic systems with lithium ion battery storage in the United States. *Renew. Sustain. Energy Rev.* **2018**, *94*, 1057–1066. [CrossRef]
24. Zhou, Y. Sustainable energy sharing districts with electrochemical battery degradation in design, planning, operation and multi-objective optimisation. *Renew. Energy* **2023**, *202*, 1324–1341. [CrossRef]
25. Han, X.; Lu, L.; Zheng, Y.; Feng, X.; Li, Z.; Li, J.; Ouyang, M. A review on the key issues of the lithium ion battery degradation among the whole life cycle. *eTransportation* **2019**, *1*, 100005. [CrossRef]
26. Edge, J.S.; O'kAne, S.; Prosser, R.; Kirkaldy, N.D.; Patel, A.N.; Hales, A.; Ghosh, A.; Ai, W.; Chen, J.; Yang, J.; et al. Lithium ion battery degradation: What you need to know. *Phys. Chem. Chem. Phys.* **2021**, *23*, 8200–8221. [CrossRef] [PubMed]
27. O'Kane, S.E.; Ai, W.; Madabattula, G.; Alonso-Alvarez, D.; Timms, R.; Sulzer, V.; Edge, J.S.; Wu, B.; Offer, G.J.; Marinescu, M. Lithium-ion battery degradation: How to model it. *Phys. Chem. Chem. Phys.* **2022**, *24*, 7909–7922. [CrossRef] [PubMed]
28. Ansean, D.; Garcia, V.M.; Gonzalez, M.; Blanco-Viejo, C.; Viera, J.C.; Pulido, Y.F.; Sanchez, L. Lithium-ion battery degradation indicators via incremental capacity analysis. *IEEE Trans. Ind. Appl.* **2019**, *55*, 2992–3002. [CrossRef]
29. Wu, Y.; Liu, Z.; Liu, J.; Xiao, H.; Liu, R.; Zhang, L. Optimal battery capacity of grid-connected PV-battery systems considering battery degradation. *Renew. Energy* **2022**, *181*, 10–23. [CrossRef]
30. Zhang, Z.; Zhou, K.; Yang, S. Optimal selection of energy storage system sharing schemes in industrial parks considering battery degradation. *J. Energy Storage* **2023**, *57*, 106215. [CrossRef]
31. Yoshida, A.; Sato, T.; Amano, Y.; Ito, K. Impact of electric battery degradation on cost-and energy-saving characteristics of a residential photovoltaic system. *Energy Build.* **2016**, *124*, 265–272. [CrossRef]
32. Montala Palau, M.; Cheah Mane, M.; Gomis-Bellmunt, O. Techno-economic optimization for BESS sizing and operation considering degradation and ramp rate limit requirement. *J. Energy Storage* **2025**, *105*, 114631. [CrossRef]
33. Sidi Lekhel, C.E.; Mbayed, R.; Nourollahi Hokmabad, H.; Husev, O.; Velihorskyi, O.; Monmasson, E. Joint sizing and energy management optimization with dynamic battery lifetime modeling in residential PV-battery systems. *Renew. Energy* **2026**, *260*, 125188. [CrossRef]
34. Li, Y.; Liu, K.; Foley, A.M.; Zülke, A.; Berecibar, M.; Nanini-Maury, E.; Van Mierlo, J.; Hoster, H.E. Data-driven health estimation and lifetime prediction of lithium-ion batteries: A review. *Renew. Sustain. Energy Rev.* **2019**, *113*, 109254. [CrossRef]
35. Fioriti, D.; Petrelli, M.; Berizzi, A.; Poli, D. Microgrid planning by stochastic multi-objective multi-year optimization with capacity expansion and non-linear asset degradation. *Sustainability* **2026**, *18*, 3785. [CrossRef]
36. Gao, D.; Hou, Y.; Yuan, Z.; Wei, Z.; Mao, J.; Kong, W.; Shu, Z.; Peng, B.; Yang, X. Multi-objective optimization of urban industrial building rooftop PV-storage systems: Integrating dynamic degradation and lifecycle carbon footprint. *Sustain. Cities Soc.* **2025**, *130*, 106615. [CrossRef]
37. Calise, F.; Figaj, R.D.; Vanoli, L. Energy and economic analysis of energy savings measures in a swimming pool centre by means of dynamic simulations. *Energies* **2018**, *11*, 2182. [CrossRef]
38. Figaj, R.; Szubel, M.; Przenzak, E.; Filipowicz, M. Feasibility of a small-scale hybrid dish/flat-plate solar collector system as a heat source for an absorption cooling unit. *Appl. Therm. Eng.* **2019**, *163*, 114399. [CrossRef]
39. Klein, S.A. *TRNSYS-A Transient System Simulation Program*; Engineering Experiment Station Report; University of Wisconsin-Madison: Madison, WI, USA, 1988; pp. 12–38.
40. Guo, X.L. Rooftop Solar PV Potential Assessment of Xuzhou Based on Roof Area. Master's Thesis, China University of Mining and Technology, Xuzhou, China, 2015.
41. Zhang, H.; Wang, L.; Li, Z. Evaluation Method and Application of Urban Building Rooftop Photovoltaic Utilization Potential. *Urban Probl.* **2017**, *2*, 33–39.
42. Mavromatidis, G.; Orehounig, K.; Carmeliet, J. Evaluation of photovoltaic integration potential in a village. *Sol. Energy* **2015**, *121*, 152–168. [CrossRef]

43. Freitas, S.; Catita, C.; Redweik, P.; Brito, M.C. Modelling solar potential in the urban environment: State-of-the-art review. *Renew. Sustain. Energy Rev.* **2015**, *41*, 915–931. [CrossRef]
44. Crawley, D.B.; Lawrie, L.K.; Winkelmann, F.C.; Buhl, W.; Huang, Y.; Pedersen, C.O.; Strand, R.K.; Liesen, R.J.; Fisher, D.E.; Witte, M.J.; et al. EnergyPlus: Creating a new-generation building energy simulation program. *Energy Build.* **2001**, *33*, 319–331. [CrossRef]
45. Wang, J.; Liu, P.; Hicks-Garner, J.; Sherman, E.; Soukiazian, S.; Verbrugge, M.; Tataria, H.; Musser, J.; Finamore, P. Cycle-life model for graphite-LiFePO$_4$ cells. *J. Power Sources* **2011**, *196*, 3942–3948. [CrossRef]
46. Solar Energy Laboratory, University of Wisconsin-Madison. *TRNSYS 18: A Transient System Simulation Program*; Solar Energy Laboratory, University of Wisconsin-Madison: Madison, WI, USA, 2017.
47. Jordan, D.C.; Kurtz, S.R. Photovoltaic degradation rates: An analytical review. *Prog. Photovolt. Res. Appl.* **2013**, *21*, 12–29.
48. Short, W.; Packey, D.J.; Holt, T. *NREL/TP-462-5173*; A Manual for the Economic Evaluation of Energy Efficiency and Renewable Energy Technologies. National Renewable Energy Laboratory: Golden, CO, USA, 1995.
49. Zheng, Y.; Shen, H.; Li, J. A techno-economic sizing method for PV/battery/grid hybrid solar systems for residential buildings. *J. Mech. Sci. Technol.* **2021**, *35*, 5245–5254. [CrossRef]
50. Ministry of Industry and Information Technology of the People's Republic of China. Standard Conditions for the Lithium-Ion Battery Industry (2021 Edition). Available online: https://www.miit.gov.cn/jgsj/dzs/wjfb/art/2021/art_a70dbc4fe99847b3b9c6e19603c072eb.html (accessed on 16 June 2026). (In Chinese)
51. Cole, W.; Karmakar, A. *NREL/TP-6A40-85332*; Cost Projections for Utility-Scale Battery Storage: 2023 Update. National Renewable Energy Laboratory: Golden, CO, USA, 2023.
52. Cole, W.; Frazier, A.W.; Augustine, C. *NREL/TP-6A20-79236*; Cost Projections for Utility-Scale Battery Storage: 2021 Update. National Renewable Energy Laboratory: Golden, CO, USA, 2021.
53. Rodriguez-Gallegos, C.D.; Yang, D.; Gandhi, O.; Bieri, M.; Reindl, T.; Panda, S.K. A multi-objective and robust optimization approach for sizing and placement of PV and batteries in off-grid systems fully operated by diesel generators: An Indonesian case study. *Energy* **2018**, *160*, 410–429. [CrossRef]
54. Ministry of Housing and Urban-Rural Development of the People's Republic of China. *GB 50189-2015*; Design Standard for Energy Efficiency of Public Buildings. China Architecture & Building Press: Beijing, China, 2015.
55. Remund, J.; Mueller, S.; Schilter, C.; Rihm, B. *Meteonorm Handbook*; Meteotest: Bern, Switzerland, 2017.

Disclaimer/Publisher's Note: The statements, opinions and data contained in all publications are solely those of the individual author(s) and contributor(s) and not of MDPI and/or the editor(s). MDPI and/or the editor(s) disclaim responsibility for any injury to people or property resulting from any ideas, methods, instructions or products referred to in the content.